Terahertz and Infrared Quantum Cascade Lasers, and Real-time Imaging

Academic and Research Staff
Professor Qing Hu

Visiting Scholars
Prof. Dayan Ban from University of Waterloo, Canada

Postdoctoral Associates
Sushil Kumar

Graduate Students
Alan Lee, Qi Qin, Allen Hsu, Wilt Kao, David Burghoff, Ivan Chan

Introduction

THz frequencies (*f* = 1-10 THz, $\hbar\omega$ = 4-40 meV, λ = 30-300 μm) remain one of the most underdeveloped frequency ranges, even though the potential applications in remote sensing and imaging, spectroscopy, and communications are great. This is mainly due to lack of coherent sources with high output power levels. The difficulty to generate THz radiation is because of the so-called "THz gap" in conventional semiconductor devices, which falls between two other frequency ranges in which solid-state sources have been well developed. One is the microwave and millimeter-wave frequency range, and the other is the near-infrared and optical frequency range. Semiconductor electronic devices that utilize oscillating conduction current $\vec{J}$ (such as transistors, Gunn oscillators, Schottky-diode frequency multipliers, and photomixers) are limited by the transit time and parasitic *RC* time constants. Consequently, the power level of these electronic devices decreases rapidly as the frequency *f* increases above 1 THz. In contrast to the electronic devices, photonic or quantum electronic devices (such as laser diodes) generate radiation by oscillating bounded dipoles (which give rise to an oscillating displacement current $\frac{\partial \vec{p}}{\partial t}$). As a result, they are not limited by the transient time and/or the *RC* time constant. However, for conventional bi-polar laser diodes, they are limited to frequencies above that corresponds to the semiconductor energy gap, which is higher than 10 THz even for narrow-gap lead-salt materials. Thus, the frequency range below 10 THz is inaccessible for the conventional semiconductor bi-polar diode lasers.

Semiconductor quantum-effect devices (which can be loosely termed "artificial atoms"), including both vertically grown quantum-well structures and laterally confined mesoscopic devices, are human-made quantum mechanical systems in which the energy levels can be chosen by changing the sizes of the devices. Typically, the frequency corresponding to the intersubband transitions is in the millimeter-wave range (ΔE ~ 1-4 meV) for the lateral quantum-effective devices, and THz to infrared for the vertical quantum wells. It is therefore appealing to develop ultrahigh-frequency devices, such as THz lasers utilizing the intersubband transitions in these devices.

In our group, we are systematically investigating physical and engineering issues that are relevant to devices operating from millimeter-wave and THz to infrared frequencies. Specifically, we are working on THz quantum cascade lasers based on intersubband transitions in quantum wells, their applications as local oscillators in heterodyne receivers, and real-time THz imaging using focal-plane array cameras. Recently, we have started a new project in collaboration with MIT Lincoln laboratory to develop high-efficiency mid-infrared quantum-cascade lasers at ~4-5 μm wavelength. This development could lead to important applications in infrared counter measures in protecting airplanes, and in sensitive infrared sensing.

Development of terahertz quantum cascade lasers

Sponsors
National Science Foundation
Grant ECS-0500925
NASA
Grant NNG04GC11G
SPO #000059778
SPO #00009674
AFOSR
Grant FA9550-06-1-0462

Project Staff
Sushil Kumar, Qi Qin, Wilt Kao, Ivan Chan, and Qing Hu, in collaboration with Dr. John Reno at Sandia National Lab.

Semiconductor quantum wells are human-made quantum mechanical systems in which the energy levels can be designed and engineered to be of any value. Consequently, unipolar lasers based on intersubband transitions (electrons that make lasing transitions between subband levels within the conduction band) were proposed for long-wavelength sources as early as the 1970s. However, because of the great challenge in epitaxial material growth and the unfavorable fast nonradiative relaxation rate, unipolar intersubband-transition lasers (also called quantum-cascade lasers) at mid-infrared wavelengths were developed only recently at Bell Laboratories. This achievement paved the way for development of coherent laser sources at customized frequencies ranging from THz to near-infrared. However, compared to the infrared QCLs, THz QCLs at much longer wavelengths face unique challenging issues. First, the energy levels corresponding to THz frequencies (1 THz = 4 meV) are quite narrow, so it is very challenging to design quantum well structures for selective injection to the upper level and selective depopulate electrons from the lower level. The requirements for fabrication of such quantum-well structures with adequate accuracies are also demanding. Because of the narrow separation between subband levels, heating and electron-electron scattering will have a much greater effect. Second, mode confinement, which is essential for any laser oscillation, is difficult at longer wavelengths. Conventional dielectric-waveguide confinement is not applicable because the evanescent field penetration, which is proportional to the wavelength and is on the order of several tens of microns, is much greater than the active gain medium of several microns. Recently (November 2002), we made a breakthrough in developing quantum-cascade lasers at 3.4 THz (corresponding to 87 μm wavelength). Since then, we have made rapid progress in developing many lasers with record performance, including but not limited to the highest pulsed operating temperature of ~170 K, highest CW operating temperature of 117 K, and the longest wavelength of 188 μm (corresponding to 1.6 THz). Key results are summarized in the following sections.

THz quantum cascade lasers based on resonant phonon scattering for depopulation

The direct use of LO-phonon scattering for depopulation of the lower state offers several distinctive advantages. First, when a collector state is separated from the lower state by at least the phonon energy $\hbar\omega_{LO}$, depopulation can be extremely fast, and it does not depend much on temperature or the electron distribution. Second, the large energy separation provides intrinsic protection against thermal backfilling of the lower radiative state. Both properties are important in allowing higher temperature operation of lasers at longer wavelengths.

The present design combines advantages of our two previously investigated THz emitters. As shown in Fig. 1, the radiative transition between levels 5 and 4 is spatially vertical, yielding a large oscillator strength. The depopulation is highly selective, as only the lower level 4 is at resonance with a level 3 in the adjacent well, where fast LO-phonon scattering takes place. The four-well structure inside the dashed box is one module of the structure, and 175 such modules are connected in series to form the quantum cascade laser.

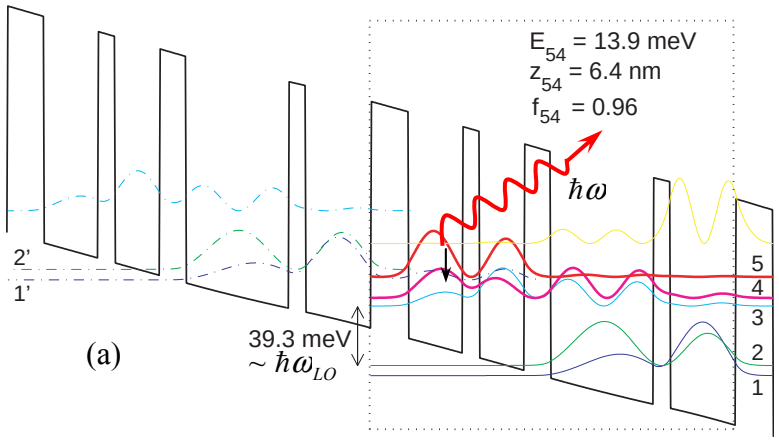

Figure 1. Conduction band profile calculated using a self-consistent Schrödinger and Poisson solver (80% conduction band offset) biased at 64 mV/module. Beginning with the injector barrier, the layer thickness in Å are **54**/78/**24**/64/**38**/148/**24**/94. The 148-Å well is doped with Si at 1.9×10^{16}/cm^3, yielding a sheet density of 2.8×10^{10}/cm^2.

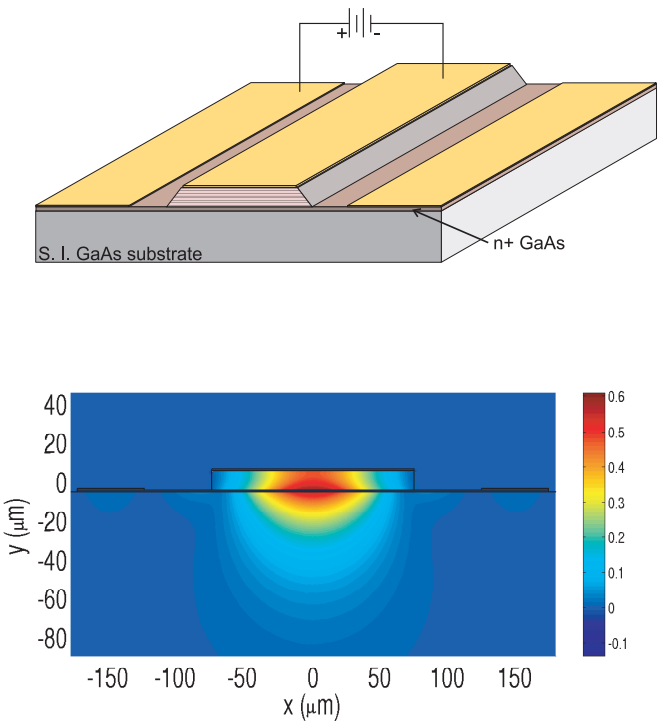

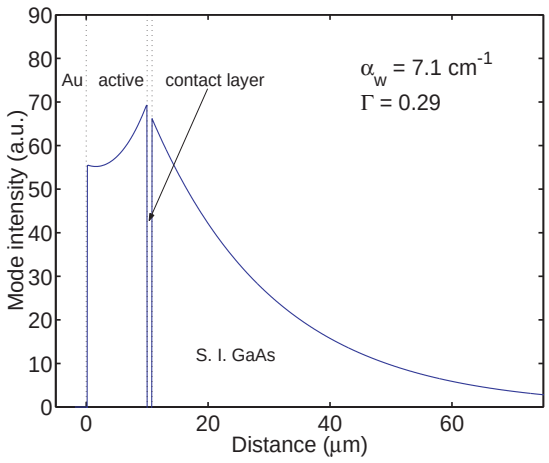

Figure 2. Schematic of the THz laser ridge structure, calculated two-dimensional mode profile using FEMLAB (on the left), and one-dimensional mode profile, confinement factor, and waveguide loss (on the right).

Mode confinement in this laser device was achieved using a surface plasmon layer grown under the active region. The schematic of the device structure and the calculated mode profile and waveguide loss are shown in Fig. 2. The calculated waveguide loss of 7.1 cm^{-1} and mode confinement factor $\Gamma \approx$ 29% are quite favorable compared to the calculated gain of our laser device. After the rear facet was high-reflection (HR) coated, lasing was obtained in this device and a typical emission spectrum above

threshold is shown in Fig. 3(a). The emission frequency corresponds to a photon energy of 14.2 meV, close to the calculated value of 13.9 meV. Pulsed lasing operation is observed up to 87 K with a power level of 13 mW at 5 K, and ~4 mW even at liquid-nitrogen temperature of 78 K, as shown in Fig. 3(b).

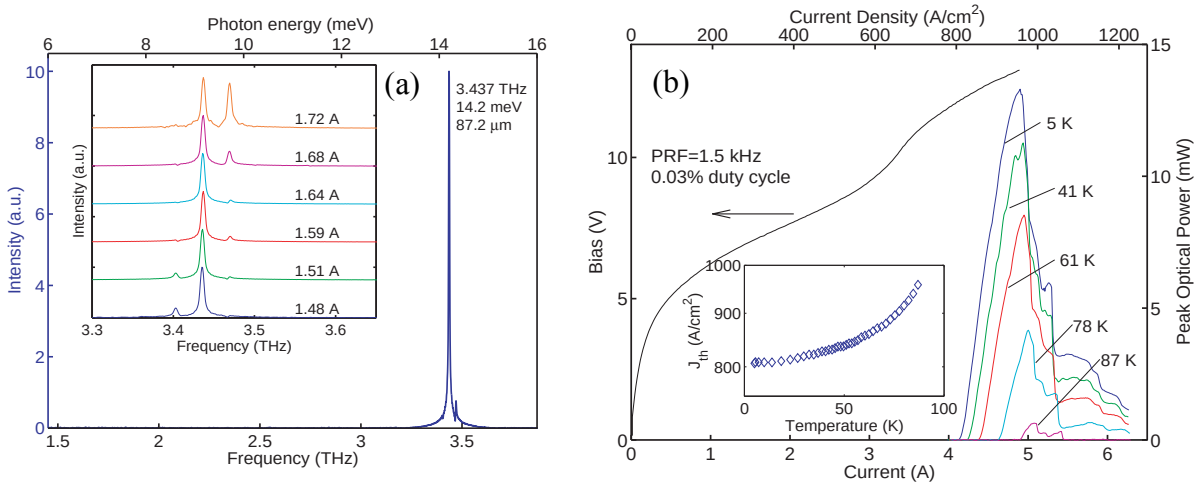

Figure 3. (a) Emission spectrum above threshold. The inset shows a set of emission spectra that are Stark-shifted to higher frequencies with higher bias. (b) Pulsed power-current relations taken from a similar laser device at different heat-sink temperatures.

THz quantum cascade lasers using metal waveguides for mode confinement

After our initial success in the development of 3.4-THz quantum cascade laser, one of the improvements made was the mode confinement. As shown in Fig. 2, the mode confinement using surface plasmon layer yields a relatively low mode confinement factor of $\Gamma \approx 0.29$. This mode confinement is sufficient for lasing at 3.4 THz. However, as we are developing even longer wavelength quantum cascade lasers, the mode confinement will become much worse or even unconfined at frequencies lower than 2 THz for the carrier concentration in our laser structures. An alternative method for mode confinement is to use metal waveguides. As shown in Fig. 4, the mode is now tightly confined between the top and bottom metal contacts, yielding a confinement factor close to 100%. Fig. 4 also shows the process of wafer bonding and selective etching to fabricate such a metal waveguide structure.

Using a combination of the metal-metal waveguides and improved gain medium, we have developed THz QCLs with many record performance in the last year. Some of the highlights of these achievements are summarized in Fig. 5, including the highest operating temperature of ~186 K in the pulsed mode (at this temperature $k_B T/\hbar\omega > 1$, which is unprecedented for any solid-state photonic devices), 117 K in CW mode, and long wavelength (207 μm, corresponding to 1.45 THz).

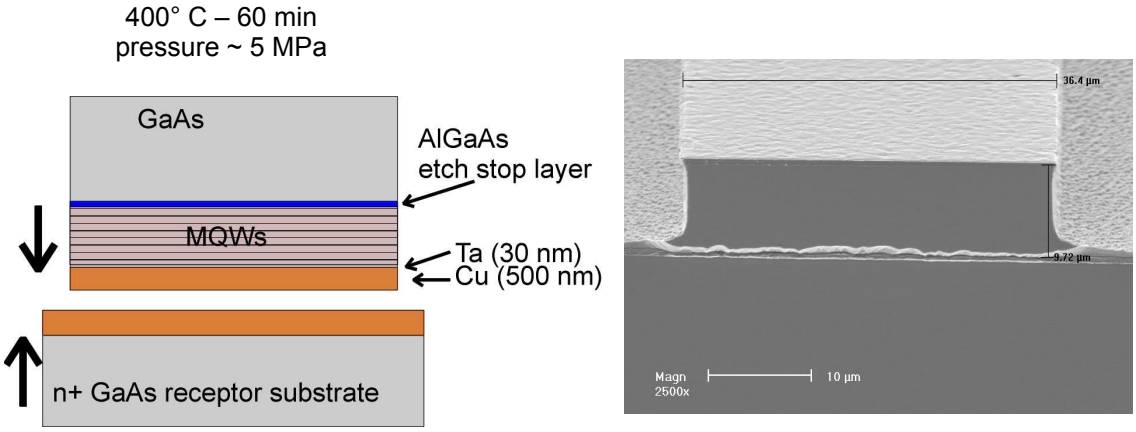

Figure 4. Left: Schematic of the wafer bonding process for double-side metal-metal waveguide. Right: A SEM picture of a fabricated device.

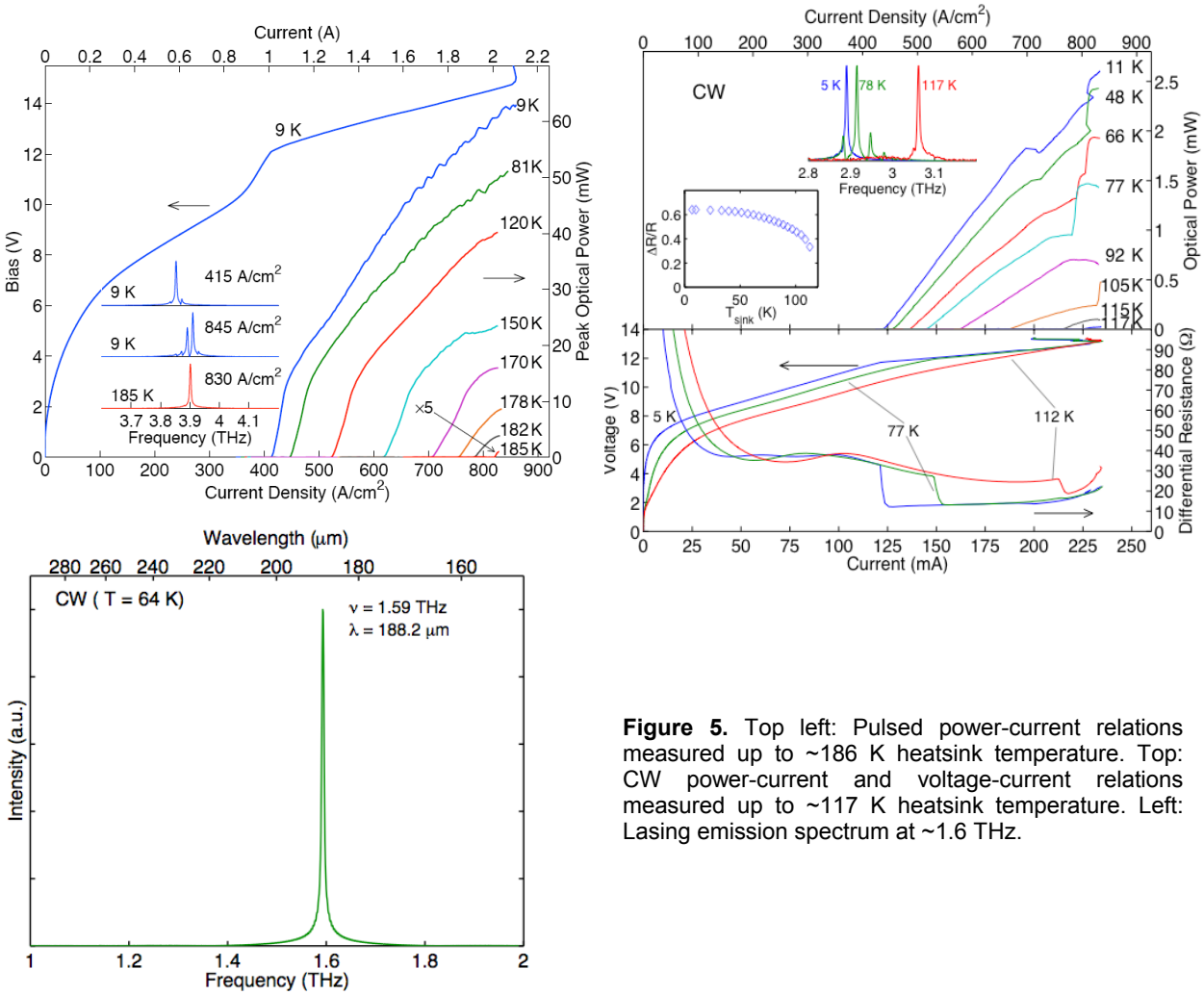

Figure 5. Top left: Pulsed power-current relations measured up to ~186 K heatsink temperature. Top: CW power-current and voltage-current relations measured up to ~117 K heatsink temperature. Left: Lasing emission spectrum at ~1.6 THz.

In addition to the record performance in operating temperatures and wavelength, we have recently developed high-power THz quantum-cascade lasers that produce ~250 mW of power, as shown in Fig. 6. Using these high-power lasers, we are now able to perform THz imaging in real time at a video rate of ~20 frames/second, that is, making movies in T-rays.

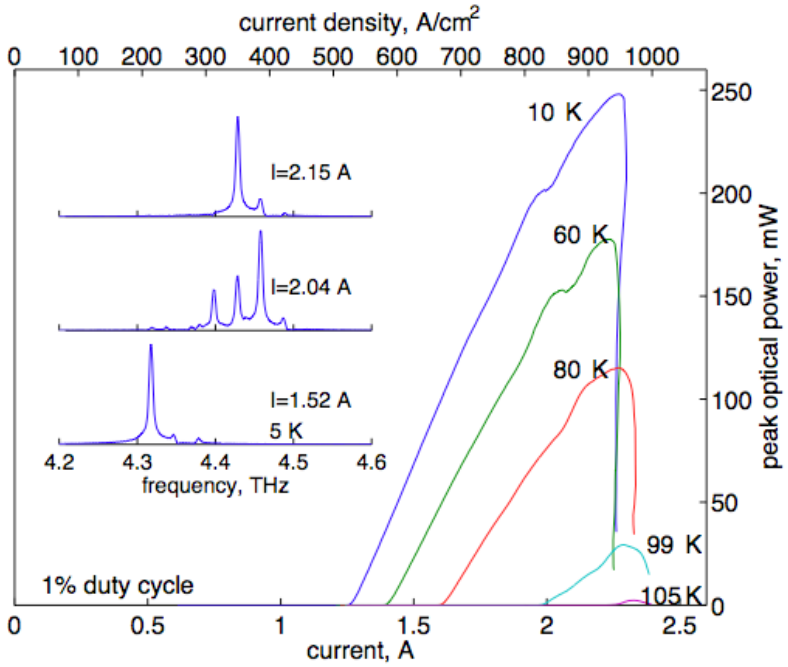

Figure 6. A 4.4-THz quantum-cascade laser with peak power level of ~250 mW.

Terahertz heterodyne receiver using QCLs and hot-electron bolometers

Sponsors
National Science Foundation
Grant ECS-0500925
NASA
Grant NNG04GC11G
SPO #000059778
SPO #00009674
AFOSR
Grant FA9550-06-1-0462

Project Staff
Ben Williams, Sushil Kumar, Wilt Kao, Ivan Chan, and Qing Hu, in collaboration with J.R. Gao, J. N. Hovenier, J. J. A. Baselmans, Z.Q. Yang, A. Baryshev, M. Hajenius, T. M. Klapwijk, A.J.L. Adam, and T.O. Klaassen at SRON National Institute for Space Research, and Kavli Institute of NanoScience Delft, Delft University of Technology, the Netherlands, and Dr. John Reno at Sandia National Lab.

The terahertz (THz) region of the electromagnetic spectrum (300 GHz – 10 THz) is the least explored spectral region in astronomy, despite the fact that it contains half the luminosity and 98% of the photons of the universe. This is mainly caused by the absence of sensitive detectors and the fact that the earth's atmosphere is opaque for large fractions of this spectral region. Ground, air and space based observatories are now starting to lift the veil but they are limited by the current state-of-the-art radiation detectors. In particular, there are no spectrometers capable of performing very high-

resolution spectroscopy above 2 THz suitable for space-based observatories. Here we report the first demonstration of an *all* solid-state heterodyne receiver that can be used as a spectrometer at frequencies above 2 THz. The system we present uses a hot electron bolometer as mixer and a quantum cascade laser as the local oscillator, operating at 2.8 THz, with an unprecedented combination of sensitivity and stability. The complete system provides a unique solution for THz spectroscopy for astronomy as well as Earth science.

Fig. 7 shows a schematic view of the experimental setup with the QCL and the HEB mounted in two separate dewars. A wideband spiral antenna coupled NbN HEB mixer is used with a superconducting bridge of 4 μm wide, 0.4 μm long, and about 4 nm thick. The normal state resistance R_N of the device, measured above the critical temperature of about 9 K, is 65 Ω. Without radiation applied a critical current I_c of 320 μA is observed at 4.2 K. The radiation is coupled to the antenna using a standard quasi-optical technique: the Si chip with the HEB is glued to the back of an elliptical, anti-reflection coated Si lens. The lens is placed in a metal mixer block thermally anchored to the 4.2 K cold plate. The divergent beam from the QCL passes through a high-density polyethylene (HDPE) dewar-window and is collimated with a parabolic mirror. The radiation is further guided to the HEB dewar through a flat mirror and a 6 μm thick Mylar beam splitter, which acts as a directional coupler. A blackbody source (of Eccosorb) is used as the signal source, which defines a hot load at 295 K and a cold load at 77 K. The signal is combined with the QCL beam through the beam splitter. Both signals pass through the thin HDPE window and a metal mesh heat filter at 77 K of the HEB dewar. The IF signal, resulting from the mixing of the LO and the hot/cold load signal, is amplified using a low noise amplifier operated at 4.2 K, and is further fed to a room temperature amplifier and filtered at 1.4 GHz in a band of 80 MHz.

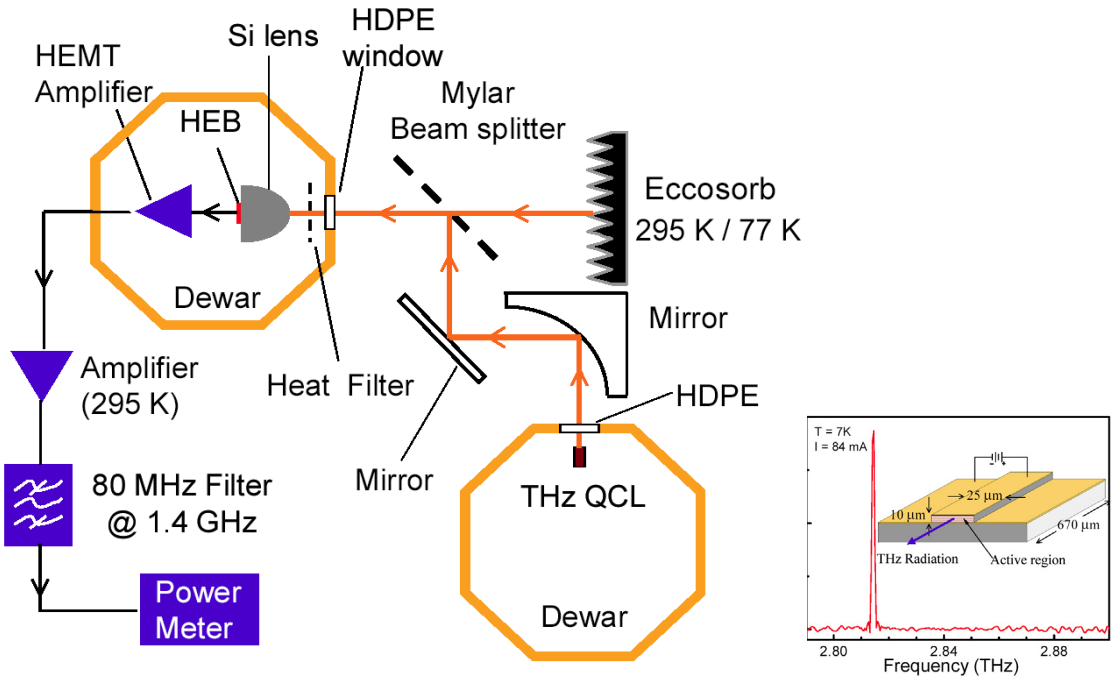

Figure 7. Schematic of the heterodyne receiver measurement set-up.

The key result of this work is demonstrated in Fig. 8. A set of current versus voltage (I-V) curves of the HEB is shown for various levels (270, 300, 330 nW) of the effective power of radiation absorbed at the HEB, together with the receiver noise temperature, $T_{N,\,rec}$, as a function of voltage. (The inset shows a top view of the HEB with its spiral antenna). The power is varied by changing the DC current of the QCL, and the level is estimated by evaluating the absorbed power by the HEB through the isothermal technique. The noise temperature $T_{N,\,rec}$ is determined from the ratio of the IF output noise power for a hot and a cold load. Each set of $T_{N,\,rec}$-V data shows a minimum region, indicating the optimum bias point. Best results are obtained for 300 nW LO power and 0.7 mV DC bias with $T_{N,\,rec}$ being as low as 1400 K, which is among the lowest obtained at this high frequency. This work, along with the phase-locking measurement described in the next section, has firmly established QCL's suitability in local-oscillator applications in a frequency range where no solid-state sources are available prior to our work.

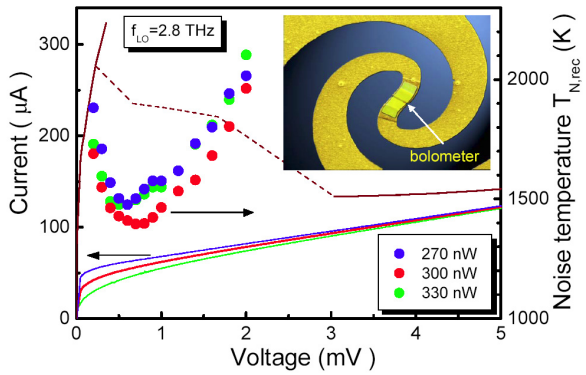

Figure 8. Current-voltage characteristics (solid line, left axis) of a NbN hot-electron bolometer (HEB) without and with radiation from a QCL at 2.814 THz. The measured receiver noise temperature $T_{N,rec}$ is shown as symbols (right axis) versus the bias voltage at different LO power levels. The inset shows a top view of the HEB with its spiral antenna.

Phase-locking of a THz quantum cascade laser to a microwave reference

Sponsors
National Science Foundation
Grant ECS-0500925
NASA
Grant NNG04GC11G
SPO #000059778
SPO #00009674
AFOSR
Grant FA9550-06-1-0462

Project Staff
Ben Williams, Sushil Kumar, and Qing Hu, in collaboration with J.R. Gao, E. E. Orlova, J. N. Hovenier, J. J. A. Baselmans, Z.Q. Yang, A. Baryshev, M. Hajenius, T. M. Klapwijk, A.J.L. Adam, and T.O. Klaassen at SRON National Institute for Space Research, and Kavli Institute of NanoScience Delft, Delft University of Technology, the Netherlands, and Dr. John Reno at Sandia National Lab.

Terahertz quantum cascade lasers (QCLs) are promising sources for various applications such as high-resolution heterodyne spectroscopy, sensing, and imaging. In particular, QCLs hold great promise for local-oscillator (LO) applications because of their demonstrated performances: a broad frequency coverage of 1.2 - 5 THz, high output power (≥1 mW), and compactness. Recently, their suitability as LOs has been demonstrated in hot electron bolometer (HEB) receivers with free-running QCLs, calibrated with a broadband blackbody radiation. To proceed with the applications of THz QCLs as LOs in a heterodyne spectrometer, stabilization of the frequency or phase is required to either eliminate the frequency jitter or to reduce the phase noise. For a heterodyne interferometer either on the Earth or in space, phase locking of multiple LOs to a common reference at low frequency is essential.

Phase locking a laser to a reference means to control the phase of the laser radiation field precisely. This serves not only to stabilize the frequency but also to transfer the line profile of the reference to the laser. In the case of frequency-locking, the laser's average frequency is fixed, but its linewidth remains equal to the laser's intrinsic linewidth. Until now, only a few experiments to stabilize a THz QCL have been published. They are the frequency locking of a 3.1 THz QCL to a far-infrared (FIR) gas laser, the phase-locking of the beat signal of a two lateral modes of a THz QCL to a microwave reference, and the phase locking of a 1.5 THz QCL to a multiplier chain LO source. These experiments have suggested the feasibility of phase-locking, but have not led to a practical scheme for a LO. For a practical solution the phase needs to be locked to an external reference that can be generated conveniently and should preferably be far below the LO frequency. Therefore, an important challenge is the demonstration of phase-locking of a single-mode THz QCL to a microwave reference signal (MRS), which is the scheme commonly used in existing solid-state LOs. The MRS should be multiplied to a THz frequency in the vicinity of the laser frequency in order to obtain a beat note or an intermediate frequency (IF). In this project, we have demonstrated the phase-locking of a 2.7-THz QCL to a harmonic generated from a MRS by a semiconductor superlattice (SL) nonlinear device in combination with a multiplier chain.

Fig. 9 shows a schematic diagram of the complete setup. The reference starts with a microwave synthesizer (Agilent 83640B) operated at 15.196 GHz followed by the multiplier chain that brings up the frequency to 182.352 GHz with a power level of 20-30 mW. The latter is used to pump the SL device to generate the 15^{th} harmonic at 2.73528 THz, which is in the vicinity of the QCL's frequency, with a power level of 1-2 pW. The QCL is biased by a DC current, supplied by a phase-lock module (XL Microwave 800A-801, typically for Gunn and YIG oscillators). The reference signal and output of the QCL are combined in the HEB mixer via a beam-splitter. The beat signal is amplified by an IF chain consisting of an isolator, a cryogenic low noise amplifier, and room temperature amplifiers.
We first monitor the beat signal of the free-running QCL by a spectrum analyzer (alternatively by a fast Fourier transform spectrometer[19]), which is connected directly to the output of the IF chain. From the spectrum we obtain the frequency of the QCL to be 2.73673 THz. With this technique we can

determine the frequency with a very high precision. By varying the current bias of the QCL the lasing frequency shifts monotonically and increases by 1.6 GHz from 30 to 46 mA (corresponding to 10.8 to 11.4 V), with the rate of 98 MHz/mA. This blue shift is most likely due to the frequency pulling of a Stark-shifted gain spectrum. The tuning mechanism which has a time constant of ~ps is much faster than the thermal tuning (>1 ms) that results in a red shift. The faster tuning allows the use of a feedback control with a broad bandwidth (~1 MHz). In essence, the QCL behaves as a voltage controlled oscillator for the bias range of interest, which is required for phase-locking. To close the phase-lock loop (PLL), the beat signal, as shown in Fig. 9, is fed into a low-pass filter and then down-converted to about 100 MHz by a microwave mixer that has a microwave source at 1.54 GHz as LO. This is technically necessary since our phase-lock module is designed for the phase comparison with a synthesized reference signal at 100 MHz. The phase error signal is fed back into DC bias to the QCL. The PLL gain bandwidth is 1 MHz. All the instruments (the spectrum analyzer and signal generators) are phase locked to a common 10-MHz reference.

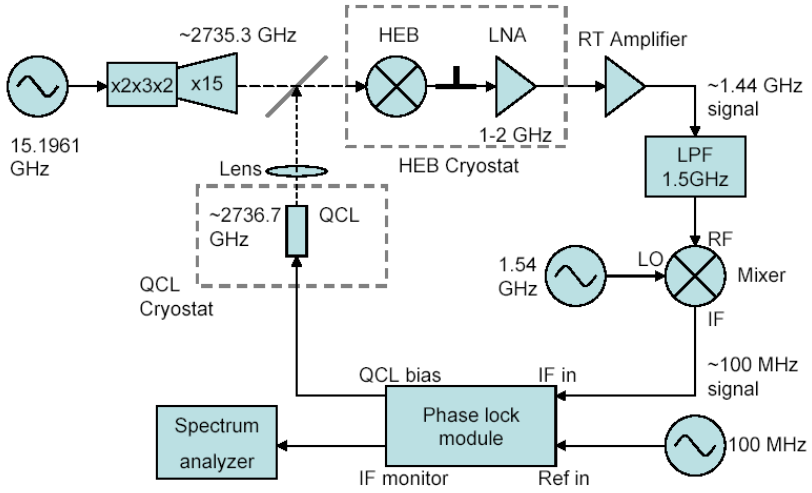

Figure. 9. Schematic diagram of the experimental setup to phase lock a THz QCL at 2.7 THz to a microwave reference. Not shown is that all the spectrum analyzer and signal generators are phase locked to a common 10-MHz reference.

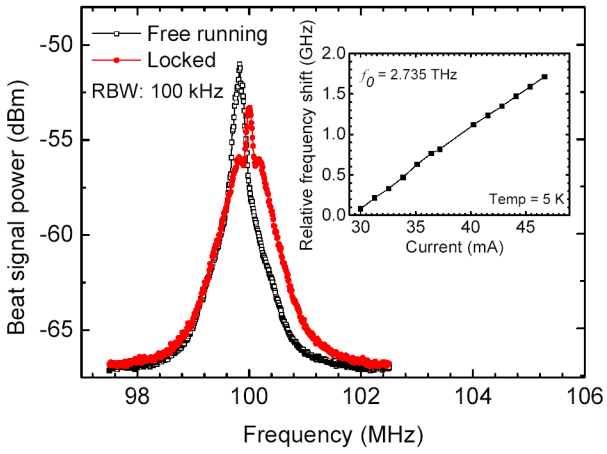

Figure. 10. A typical power spectrum of the beat signal of the THz QCL that is phase locked to a microwave reference recorded by the spectrum analyser with a low resolution bandwidth (RBW) of 100 KHz. For comparison, a spectrum of the free-running QCL is also shown. The inset shows a relative frequency shift of the free- running QCL versus the biasing current at 5 K. The starting frequency is 2.735 THz.

Real-time terahertz imaging using a microbolometer focal-plane array camera

Sponsors
National Science Foundation
Grant ECS-0500925
NASA
Grant NNG04GC11G
SPO #000059778
SPO #00009674
AFOSR
Grant FA9550-06-1-0462

Project Staff
Alan Lee, Ben Williams, Sushil Kumar, Qi Qin, and Qing Hu

Imaging using radiation in the terahertz frequency range, 0.3 THz to 10 THz, has demonstrated the ability to see the details within visibly opaque objects such as: integrated circuits packages, leaves, teeth, thin tissue samples, and illicit drugs in envelopes. The vast majority of THz imaging has been done by linearly scanning an object through a tightly focused THz beam – a practice which limits the acquisition time to the mechanical scan rate of the system. With upper limits of 100's of pixels/second for mechanical scanning, a complete image takes minutes to acquire.

Real-time imaging (30 frames per second or more) has previously been demonstrated by using an electro-optic crystal for frequency upconversion so that THz images can be viewed with a CCD focal-plane camera. However, this setup requires precise timing of the optical and THz pulses, necessitating a scanning delay mechanism, adding to its complexity. Furthermore, because of the short THz pulses (<1 ps), this scheme is inherently broadband (>1 THz). In applications such as the drug detection scheme, where detection of narrow-band fingerprint is required, a coherent narrow-band illumination source is crucial. Due to their compact sizes, many THz quantum-cascade lasers with different frequencies, corresponding to different chemical absorption bands, can be packaged tightly, forming a frequency agile coherent radiation source. In combination with a focal-plane imager, such a system can perform frequency-sensitive THz imaging at a rate far greater than the previous methods, allowing real-time THz monitoring and screening.

In this work, real-time, continuous wave (CW) terahertz imaging is demonstrated for the first time using THz QCLs and a focal-plane array camera. The experimental arrangement is shown in Fig. 11. The terahertz QCL is cooled by a cryogen-free pulsed-tube thermomechanical cooler, produces ~50 mW of power at ~30 K. As shown in the figure, imaging experiments in both transmission and reflection mode can be performed. Since the microbolometer camera was initially designed for the 10-μm wavelength range for night-vision applications, we developed a differential scheme to subtract the strong ambient background at ~300 K and reduce 1/*f* noise.

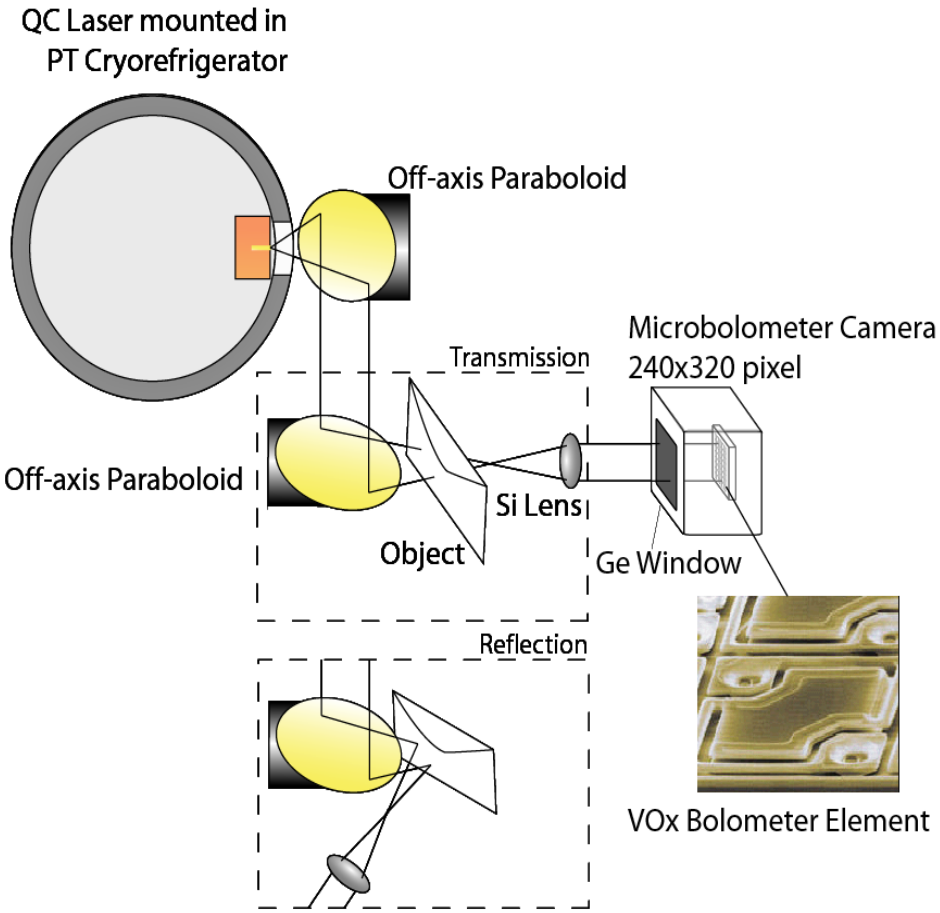

Figure. 11. Experimental setup of the THz imaging system. The photo shows a vanadium oxide microbolometer (Courtesy of BAE Systems, Lexington, MA). Cutaway depicts alternate reflection mode setup

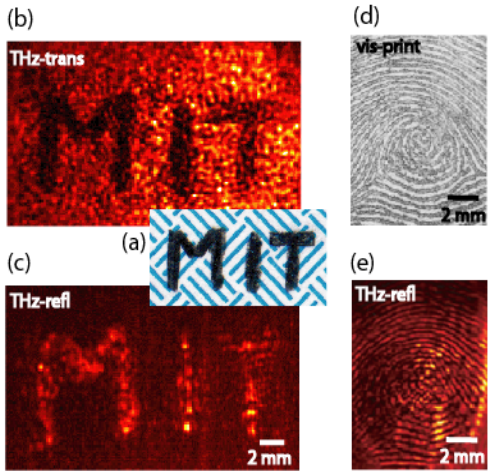

Figure. 12. Pencil letters written on the inside of a paper security envelope at visible frequencies (a), in THz transmission mode (b, 1 frame, 1/20 second) and THz reflection mode (c, 20 frames, 1 second). Visible frequency thumb print (d), and THz reflection mode image the thumb of the leading author (e, 20 frames).

Recently, we demonstrated the use of a terahertz (THz) quantum cascade laser (QCL) for real-time imaging in transmission mode at a standoff distance of 25 meters. The lasing frequency was selected for optimum transmission within an atmospheric window at ~4.9 THz. Coarse frequency selection was made by design of the QCL gain medium. Finer selection (to within 0.1 THz) was made by judicious choice of laser cavity length to adjust the facet loss and therefore the lasing threshold bias, in order to overlap the peak frequency of the Stark-shifted gain spectrum with the atmospheric window.

Due to the distinctive THz spectral "fingerprints" found in many chemical compounds, THz sensing and imaging could have important military and security applications. For these applications, imaging at a standoff distance (~10-25 meters) is essential. However, water vapor strongly absorbs radiation at THz frequencies, which results in heavy atmospheric attenuation, >10 dB/m, outside of isolated low-loss transmission windows, which are only a few hundred GHz wide. These narrow transmission bands favor the use of narrowband sources. Far-infrared gas lasers are bulky and power hungry, and they have only limited selection of lasing frequencies. Schottky-diode frequency multipliers can only produce sub-milliwatt power levels at f > 1 THz, and are not suitable for illuminating focal-plane arrays for real-time imaging. By comparison, THz QCLs have demonstrated peak power levels of ~250 mW in pulsed and ~130 mW in CW operations. Their intersubband-transition nature implies that any desired frequency can be achieved by bandgap and waveguide engineering over a continuous frequency range from 1.59 to 5 THz, over which these lasers have been demonstrated. In this, we demonstrate the use of a frequency optimized THz QCL for real-time imaging in transmission mode over a standoff distance of 25.8 meters.

The experimental set-up for long-range imaging is shown in Fig. 13. The emitted light was collected and collimated by an f/1 off-axis parabolic mirror with a 5-cm diameter. In configuration (1), an f/3, high-resistivity Si lens was used to focus the light transmitted through an object placed at 2 meters in front of the spherical mirror, onto a 320×240 microbolometer focal plane array (optical NEP ~ 320 pW/√Hz at 4.3 THz). Note that in the object plane, which is ~23-meters from the laser source, the beam pattern is highly symmetric as measured by the focal-plane array camera with 1-second integration time. In configuration (2), the reflected beam from the spherical mirror was further focused by an f/2 off-axis parabolic mirror and was used to back illuminate a smaller object. Transmitted light was collected and focused by an f/1 high-resistivity Si lens onto the focal plane array.

The resulting images are shown in Fig. 14. A dried seed pod is used as the see-through object to simulate foliage penetration (FOPEN). In part (a) a white light image of the dried seed pod is shown,

with the corresponding THz transmission images shown in parts (b) and (c) for configurations (1) and (2) respectively. After transmission over the 25.75-m path, the resulting focal-plane average SNR was ~2.5 and 10, for a single-frame and a 20-frame average (0.05 and 1 second of integration, respectively) respectively. The 20-frame average images shown in (b) and (c) were normalized to the beam pattern and were spatially low-pass filtered to smooth out isolated pixels with low SNR. This post detection signal processing is performed in real time, and only adds a ~5-ms delay in displaying the images. The image in part (b) has low spatial resolution due to the 2-meter distance from the spherical mirror. Part (c) shows a much higher spatial resolution, due to the closer positioning of the object to the camera. As a result, the fine ridges of the seed pod (~millimeter spacing) can be resolved, as predicted by the ray tracing resolution of ~0.75 mm.

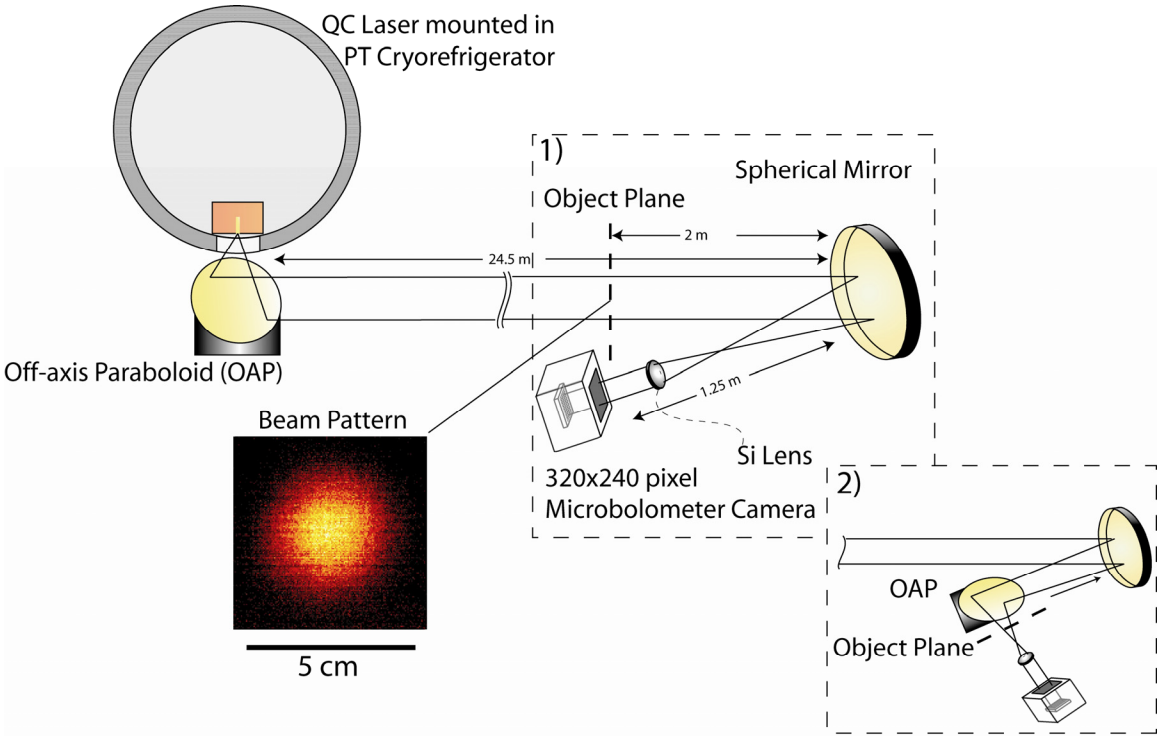

Figure 13. Experimental setup for imaging over a distance of 25.75 meters. A QCL device is mounted in a pulse-tube cryocooler, with emitted beam collimated by an off-axis paraboloid mirror, for transmission over a 24.5-m path before collection by a 15-cm diameter spherical mirror. In configuration (1), an object is placed 2 meters before a spherical mirror; in configuration (2), an object is placed after a second off-axis paraboloid mirror. Also shown is the beam pattern for configuration (1), measured at ~23 meters from the laser source and taken with a 320×240 element focal-plane array camera with 1-second integration.

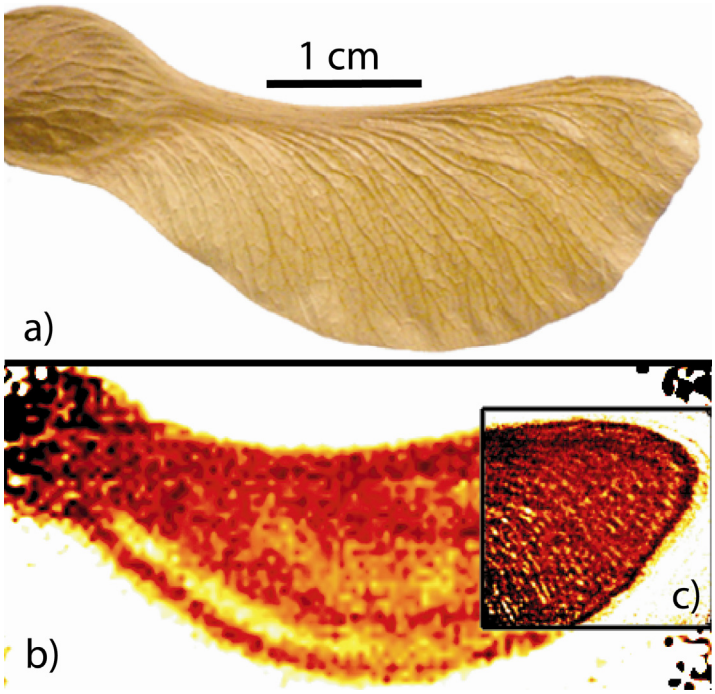

Figure 14. Sample images of a dried seed pod: (a) image at visible frequency; (b) terahertz image taken with configuration (1); (c) terahertz image taken with configuration (2). Both (b) and (c) are taken with 1-second integration (average of 20 frames).

Surface-emitting THz quantum-cascade lasers using 2nd-order DFB gratings

Sponsors
National Science Foundation
Grant ECS-0500925
NASA
Grant NNG04GC11G
SPO #000059778
SPO #00009674
AFOSR
Grant FA9550-06-1-0462

Project Staff
Sushil Kumar, Ben Williams, Qi Qin, and Qing Hu, in collaboration with Dr. John Reno at Sandia National Lab.

The metal-metal waveguides, shown in Fig. 4, have several important advantages at THz frequencies in terms of high mode confinement factor and low cavity losses. However, because of the small dimensions of the facet (~10 μm) compared to the wavelength (~100 μm), the beam pattern for edge-emitting ridge lasers are quite divergent. As a result, the facet reflection is quite high (>80% at frequencies below 3 THz), which results in a low output power level. Both features are drawbacks of the metal-metal waveguide lasers for high-power applications with good beam patterns. The surface-plasmon on semi-insulating substrate waveguides produce higher output power levels and better beam patterns because of their looser mode confinement. However, their waveguide losses are much higher, likely due to dopant absorption (both inter-impurity transitions and donor ionization frequencies are in THz) in the nominally semi-insulating substrate where a large fraction of the mode ($1-\Gamma$) resides. As a result, the thresholds are higher and the maximum operating temperatures are far lower than those of metal-metal waveguide lasers. In our recently developed high-power THz QCLs

based on surface-plasmon on semi-insulating substrates, even though the pulsed power levels are as high as ~250 mW and CW as high as ~135 mW at ~10 K, the maximum CW operating temperature is below 40 K.

It will be highly desirable to develop waveguide structures that preserve the advantage of tight mode confinement in the metal-metal waveguides, but produce higher output power levels and better beam patterns. The best solution is to use second-order distributed feedback (DFB) gratings to construct surface-emitting lasers. The schematic of which is shown in Fig. 15. Since the selection rule of intersubband transition dictates that the generated electric field is normal to the quantum-well planes (the ***y***-direction in Fig. 15), the waves will propagate along the ***z***-direction for unpatterned surface, resulting in an edge-emitting laser structure. With patterned metallic grating structures, the electric field lines will "bend" and have components in the ***z***-direction, allowing surface emission in the ***y***-direction, as illustrated in Fig. 17. The lower left panel of Fig. 15 shows that the lasing frequency can be chosen by the grating period Λ. For the second-order DFB lasing condition $\Lambda = \lambda_s$ (the wavelength in the semiconductor), the field at all apertures are in phase, resulting in a surface emission at the normal angle. It is clear that the diffraction limit for the surface-emitting structures is no longer determined by the facet dimensions; rather, it is determined by the surface dimensions which can be made much greater than the wavelengths. As a result, much narrower and symmetric beam patterns can be generated, as illustrated in the right panel in Fig. 15. Furthermore, now the coupling coefficient (output power/power inside the cavity) can be easily controlled by the filling factor of the apertures, we can couple more power out at a modest cost of slightly higher lasing thresholds. Last but not least, this structure is a DFB in nature, allowing a robust single-mode operation.

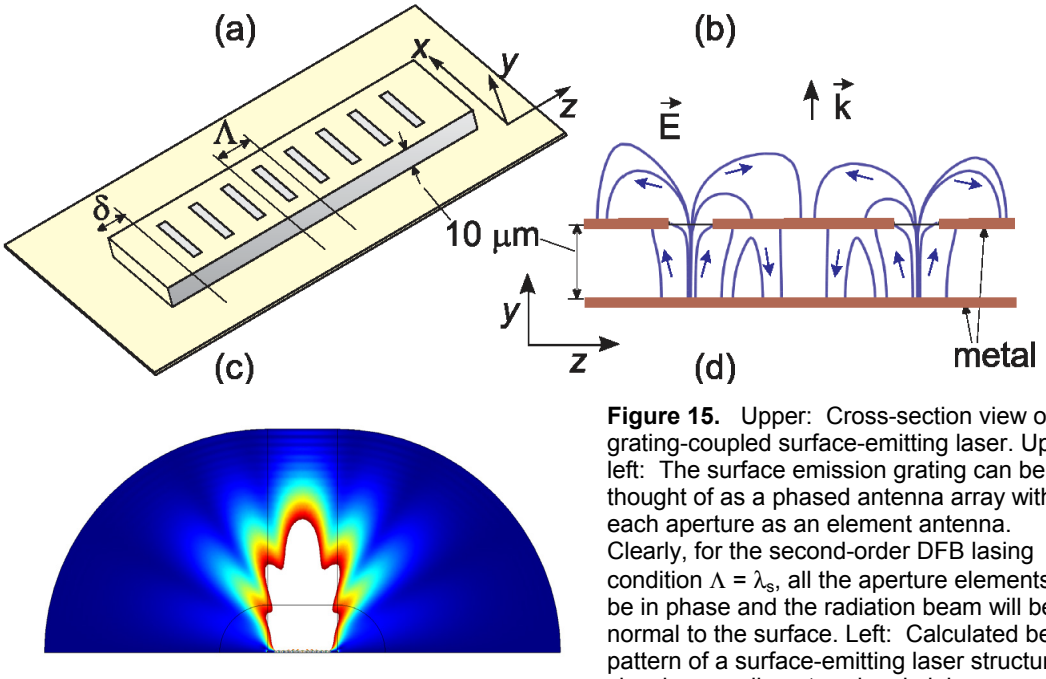

Figure 15. Upper: Cross-section view of a grating-coupled surface-emitting laser. Upper left: The surface emission grating can be thought of as a phased antenna array with each aperture as an element antenna. Clearly, for the second-order DFB lasing condition $\Lambda = \lambda_s$, all the aperture elements will be in phase and the radiation beam will be normal to the surface. Left: Calculated beam pattern of a surface-emitting laser structure, showing a well-centered main lobe.

After an extensive effort, we have developed a fabrication process so that we can coat all the sidewalls with dielectrics and metals which prevent higher-order lateral modes from lasing. SEM pictures of several devices are shown in Fig. 18, with both the extra facet lengths and central phase shift highlighted. The former helps to maintain a robust single-mode operation and the latter for a single-lobe far-field beam pattern.

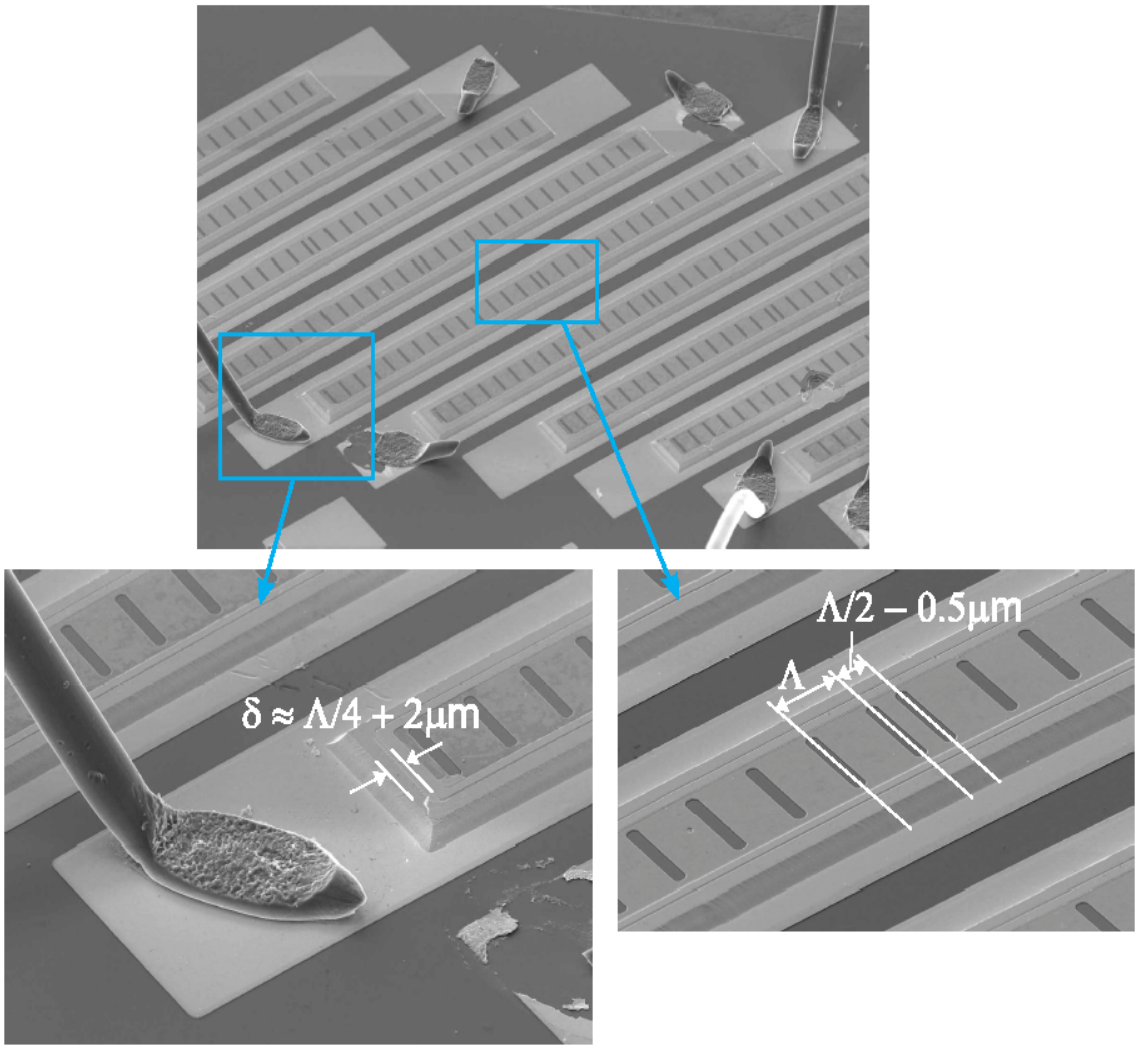

Figure 16. SEM pictures of grating-coupled surface emitting THz QC lasers.

The measurement results are summarized in Fig. 17. As can be seen, the grating-coupled surface-emitting THz QC lasers yield robust single-mode operations over a frequency range >0.3 THz. The maximum operating temperature of grating-coupled laser devices are only marginally lower than their Fabry-Perot counterparts. The beam patterns are more convergent and with a single central lobe. The power level, at ~6 mW, is more than a factor of two higher than that measured from Fabry-Perot lasers with comparable areas. This work has clearly demonstrated viability of surface-emitting scheme in terms of greater power levels, better beam patterns, and single-mode operations.

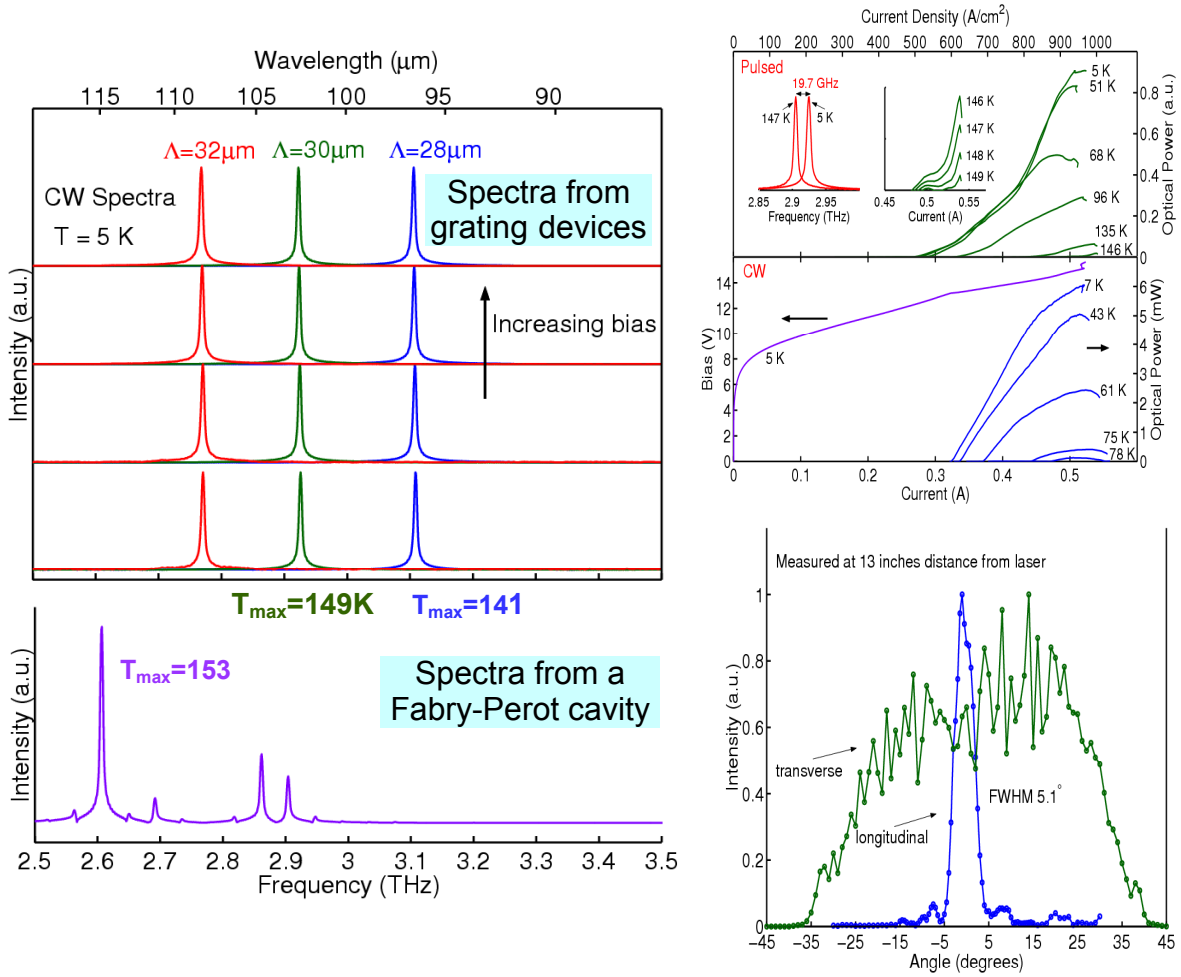

Figure 17. Upper left: Spectra from grating-coupled surface-emitting lasers. Lower left: Spectrum from Fabry-Perot laser device. Upper right: light-current and voltage-current relations of grating devices. Lower right: Measured far-field beam pattern of a grating-coupled device.

Tunable THz wire lasers

Sponsors
National Science Foundation
Grant ECS-0500925
NASA
Grant NNG04GC11G
SPO #000059778
SPO #00009674
AFOSR
Grant FA9550-06-1-0462

Project Staff
Qi Qin, Ben Williams, Sushil Kumar, and Qing Hu, in collaboration with Dr. John Reno at Sandia National Lab.

A laser device, similar to a musical instrument such as the violin, generates signals at specific frequencies. A laser whose frequency is tunable over a broad range is immensely useful in wide-

range applications including sensing, spectroscopy, and communications. In a violin, without changing parts, the frequency (pitch) can be changed by only two ways: altering the length and the tension of a string. Similarly, a conventional tunable laser's frequency is tuned only by changing the effective length (the longitudinal component of wave vector) and the refractive index (equivalent to the tension of a violin string). Here, we demonstrate a new tuning mechanism that qualitatively differs from all the other methods. Figuratively, this tuning mechanism would correspond to varying the thickness of a violin string. This is possible because of a unique feature of an unusual device termed "wire laser," whose cross section is much smaller than the wavelength. As such, the laser field extends well outside the solid waveguide core, allowing its effective thickness and consequently the frequency to be varied by direct manipulation of the evanescent mode.

In this work, the novel tuning mechanism is achieved at terahertz (THz) frequencies, where sensing and imaging applications are especially attractive based on the distinctive spectral fingerprints of many important biological and chemical species, and for which tunable lasers are essential components. However, at THz frequencies, the long wavelengths (λ~100 μm) compared to the cross section w make it difficult to implement the commonly used method of external-cavity grating for tuning. Instead of fighting the battle with brute force, the new tuning mechanism demonstrated here actually takes advantage of the small cross section relative to the wavelength, and is achieved in the extreme limit $w/\lambda << 1$ of wire lasers. Continuous frequency tuning, free of mode hopping, has been demonstrated with single-mode operation. The achieved tuning range of ~3.6% (~137 GHz) is unprecedented for any solid-state THz lasers.

The novel tuning mechanism of laser frequency demonstrated here applies to wire lasers at any frequencies. For example, one can envision such a tunable nanowire laser at visible frequencies for spectral measurements with nanometer spatial information. For THz wire lasers, further development based on MEMS (Micro-Electro-Mechanical Systems) technology will allow a finer tuning over a much greater frequency range. Such broadly tunable laser sources will have a significant impact on science and technology at THz frequencies.

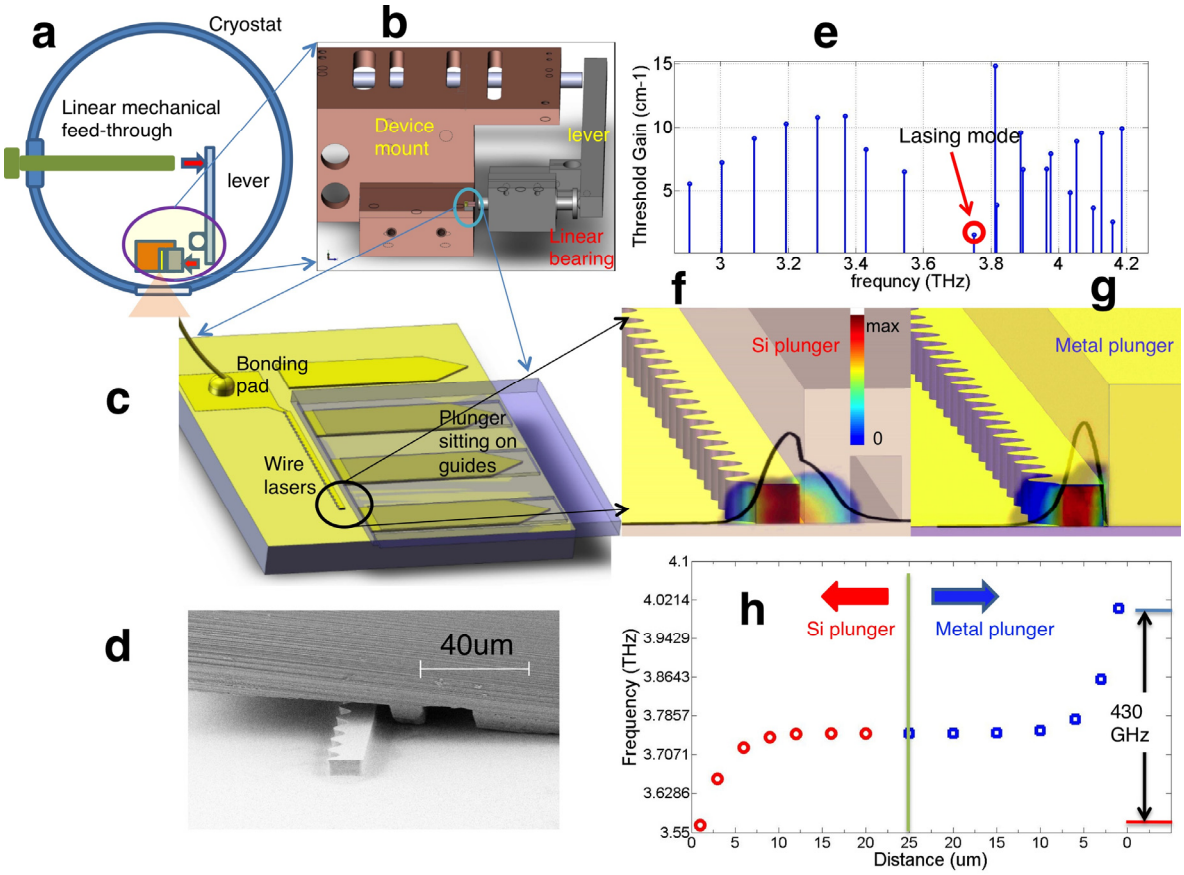

Figure 18. a, Schematic of the experimental set-up, in which a differential micrometer is used to push the long end of a lever, whose short end in turn pushes a plunger. In an alternative scheme which is not shown here, a piezoelectric transducer (PZT) inside the cryostat is used to directly push the plunger. **b,** 3D structure of device mount (copper color) and mechanical module (silver color), showing the device is mounted in the lower-right corner. **c,** Blow-up view of the device region in **b**, showing the plunger (transparent blue) residing on top of guide rails, and is ready to be actuated by the shaft of a linear bearing. Yellow color represents metal parts. **d,** SEM image of an assembled device with a silicon plunger. The average width of the laser ridge is 12.5 μm and the width of the silicon plunger is about 13 μm. To show the configuration clearly, the silicon plunger is shorter than the laser ridge so the front facet can be seen. In actual measurements, the plunger is longer, covering the entire laser ridge. **e,** Grating mode spectra of a DFB device. The laser ridge has 12.5 μm average width, 3 μm sinusoidal grating modulation, 30 periods and 13.7 μm periodicity. Plotted is the radiation loss from the open facet. This open facet is chosen at the widest location to select the fundamental upper-band-edge mode as the lasing mode, as highlighted by the red circle. **f** and **g**, Schematics illustrating the tuning mechanism with Si plunger and metal plunger respectively, with a gap of ~1 μm. The electrical-field profile is shown at the narrowest cross section of the DFB structure. The dark curve is the mode profile by integrating the electrical-field component vertical to the ground plane. By squeezing or extending the lateral mode, the metal or silicon plunger can tune the frequency to the blue or red side of a stand-alone laser. The cave in the silicon plunger is used to define the width of this plunger to be ~13 μm. This relatively small width is essential to assure a sufficient mode overlap with the gain medium to achieve lasing. **h,** Calculated lasing frequency as a function of the distance of the plunger to the device. The blue and red colors correspond to the blue and red shift of frequency. As can be seen in the figure, most of the tuning, either with the silicon or metal plunger, occurs within ~5 μm gap distance.

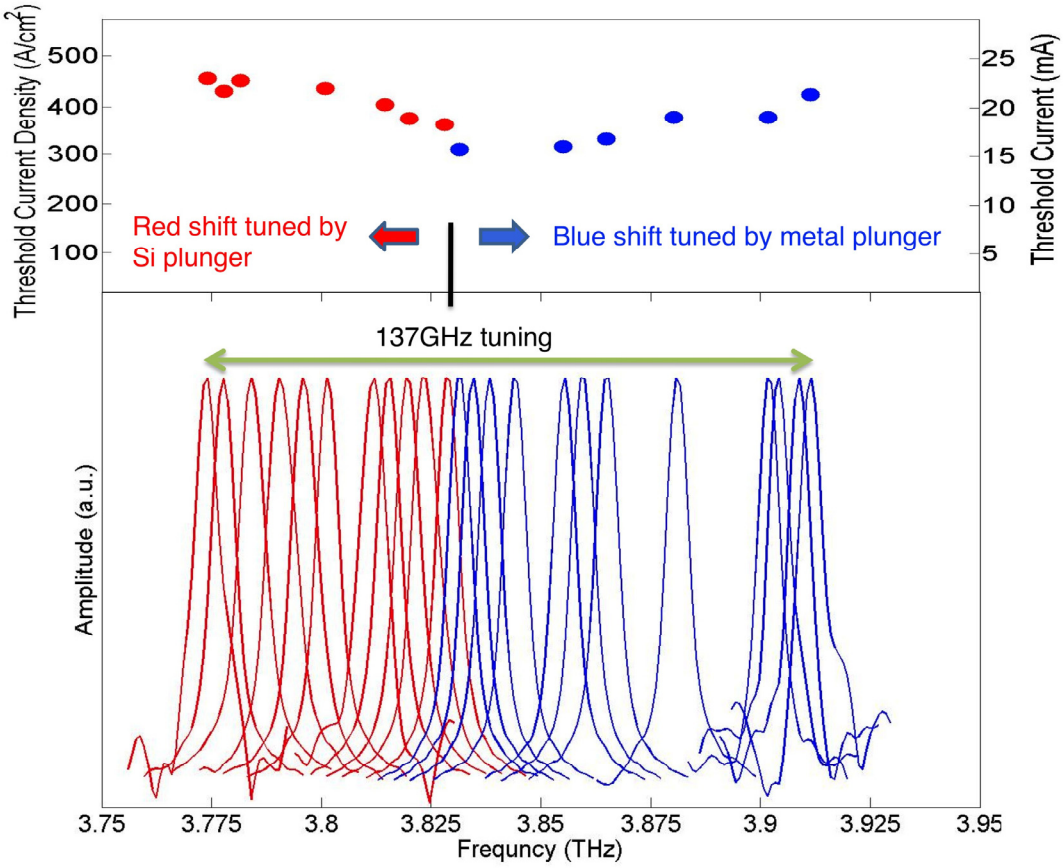

Figure 19 | **Tuning results from device T114.** The blue and red colors indicate the blue shift of frequency tuned by a gold plunger and red shift by a silicon plunger. In the upper part, plotted are the threshold current densities of the device at different frequencies, which show a moderate increase as the plunger is pushed towards the laser ridge. The lower part shows a broadband tuning of this device over a range of 137 GHz. All the spectra were recorded under the same drive current and temperature conditions. The small discontinuity is due to the stick-slip effect.

Investigation of THz quantum cascade lasers in strong magnetic fields

Sponsors
National Science Foundation
Grant ECS-0500925
NASA
Grant NNG04GC11G
SPO #000059778
SPO #00009674
AFOSR
Grant FA9550-06-1-0462

Project Staff
Ben Williams, Sushil Kumar, and Qing Hu, in collaboration with Dr. John Reno at Sandia National Lab, and Dr. Dmitry Smirnov at National High Magnetic Field Laboratory

In a terahertz QCL, the photon emission energy is smaller than the longitudinal-optical (LO) phonon energy in the semiconductor material of the QW. In the "resonant-phonon" design scheme, the population inversion is ensured by selectively injecting electrons through resonant tunneling into the upper state of the laser transition; relaxation from the lower radiative state occurs on a sub-picosecond time scale into the injector states via LO-phonon emission, this scheme has the highest operation temperature of any THz QCL design to date of T_{max}=186 K.

In THz QCLs, to achieve high-temperature operation is difficult, as the temperature increases, electrons in the upper radiative state gain sufficient in-plane energy to emit an LO-phonon, which results in a fast thermally activated scattering process, and a gain reduction. The use of 0D confinement in quantum cascade structures has been proposed as a mechanism to suppress nonradiative intersubband/level relaxation and achieve lower threshold and higher temperature operation. Although appropriate technology does not exist at this time, a magnetic field is an effective tool to analyze and improve the performance of MIR and THz QCLs in the 0D limit. A magnetic field changes the 2D parabolic energy dispersion of each size-quantized subband $\varepsilon_n(k)$ into a set of discrete, equidistant, 0D-like, Landau levels (LLs), $\varepsilon_{n,N} = E_n + (N + 1/2)\hbar\omega_c$, separated by the cyclotron energy $\hbar\omega_c = \hbar eB/m^*$, where *n* is the subband index, *N* is the LL index, *B* is the magnetic field, and *m** is the energy dependent electron effective mass. As a result, both radiative and non-radiative transitions are either reduced or resonantly enhanced by the inelastic (LO-phonon assisted) or (quasi)-elastic (interface roughness, acoustical phonons, or impurities) scattering between different LL states. Here we exploit this approach of "Landau level engineering" to explore the ultimate limits of THz QCL operation.

In summary and the figures below, we report on strong, magnetic field assisted, multi-wavelength emission in a quantum cascade laser. By applying the appropriate electrical and magnetic field, we achieve 3THz (1THz) laser emission at temperatures up to 225K (215K) at 19.3 T (31T), or change the emission frequency in an unprecedented range from 0.68THz to 3.33THz. This is the longest wavelength, the widest spectral coverage, and the highest operational temperatures of any single THz solid state laser to date. Furthermore, these results bear out the prediction that lateral quantum confinement, provided either magnetically, electrostatically, or structurally (i.e. a quantum box), is a route to higher temperature operation for THz QCLs.

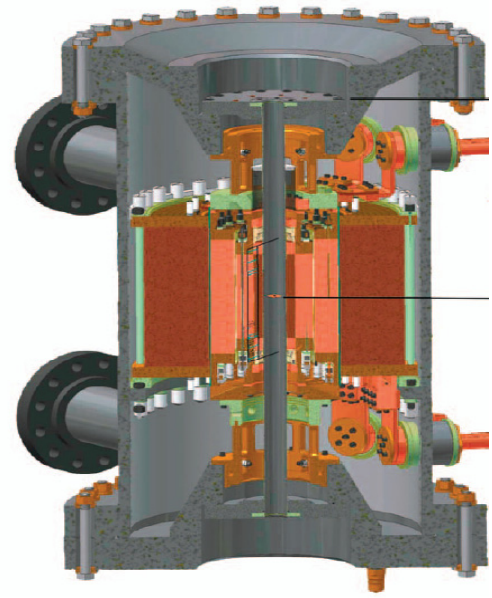

Efficient mid-wave infrared lasers (EMIL)

Sponsors
Defense Advanced Research Project Agency
Contract PO NO. 3119471

Project Staff
Allen Hsu, David Burghoff, Xinpeng Huang, Sushil Kumar, and Qing Hu, in collaboration with Dr. George Turner at MIT Lincoln laboratory and Prof. Ben Williams at UCLA.

The original invention of quantum-cascade lasers in 1994 opened up a broad electromagnetic spectrum where solid-state laser sources were underdeveloped. Slightly over ten years later, QCLs are now developed over two decades of frequency range from THz to infrared. There are many potentially important applications in this broad frequency range. One of them is infrared counter measures (IRCM) to protect airplanes from heat-seeking missiles in the atmospheric window of 3-5 μm wavelength. This project was started under the sponsorship of DARPA, along with Dr. Turner's group at MIT Lincoln Laboratory, . The goal is to develop mid-infrared quantum-cascade lasers with high wall-plug power efficiency of 50% at room temperature in the CW mode. Those lasers will

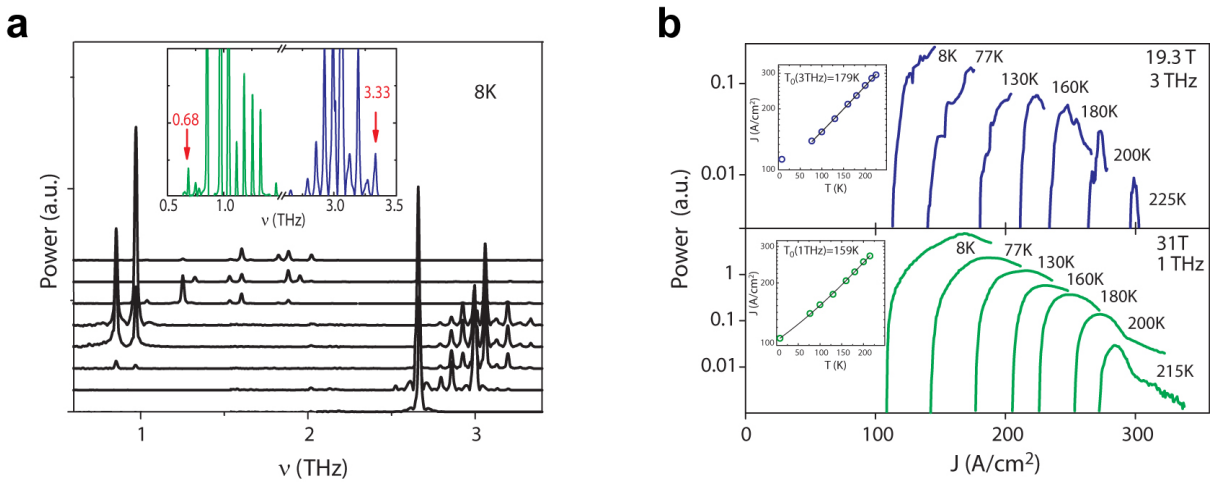

Figure 20. QCL device performance in terms of spectral coverage and operational temperature.

Top, Schematic and picture of the experimental set-up including a high-field cryostat and a FTIR spectrometer.

a, Spectral coverage of the QCL device with increasing voltage bias and magnetic field (bottom curve 54.9mV/period, 13T; top curve 88.4mV/period, 25T). The inset shows the QCLs spectral extremes: 0.68THz (69.9mV /period, 31.2T) and 3.33THz (63.9mV/period, 19T)**.**

b, Temperature dependence of *P*(*J*) at two enhanced lasing positions at 19.3T and 31T. The inserts show the current density threshold as a function of the temperature. 1THz lasing has been omitted from the 19.3T curves for visual clarity.

produce more than 1-W output power and with diffraction-limited beam patterns. Such high-efficiency and high-power solid-state diode lasers could find immediate applications in IRCM. In combination with external gratings and packaging systems that are well developed in the telecom industry, those lasers could enable compact and broadly tunable laser systems. Such a system will be quite useful in biochemical sensing for both military/security and medical/environmental applications.

With more than a decade of experience in the development of quantum-cascade lasers, our team has unique advantages in pursuing this challenging, but highly rewarding project Many numerical simulation codes, such as the Monte Carlo code, can be easily modified for the infrared quantum-cascade lasers. Such a numerical code will allow us to explore many new and different designs before going through the full process of growth and fabrication. The Lincoln Lab group has many years of experience in working on high-power infrared lasers (Sb-based), and it has close interaction with the Air Force end users of IRCM.

In order to achieve the objective of high wall-plug efficiency, we will pursue the following aspects:

- Developing robust quantum-cascade gain medium with high voltage efficiencies.
- Reducing waveguide loss to improve external power extraction efficiency.
- Fabricating narrow (~2 μm) laser ridges using ICP, incorporating InP regrowth and Au electroplating to improve heat removal for robust CW operations.
- Beam combining using external gratings to achieve high-power and broadband output.

In Fig. 21, we illustrate the band diagram and wavefunctions of a 4.7-μm QC laser based on the simplest design, with only 4 quantum wells per module. Fig. 21 also illustrates the mode profile of a 2-μm-wide laser ridge with InP regrown cladding layer and top Au layer. This simply design, termed "injectorless design" in literature, offers the advantage of higher voltage efficiency and low lasing thresholds.

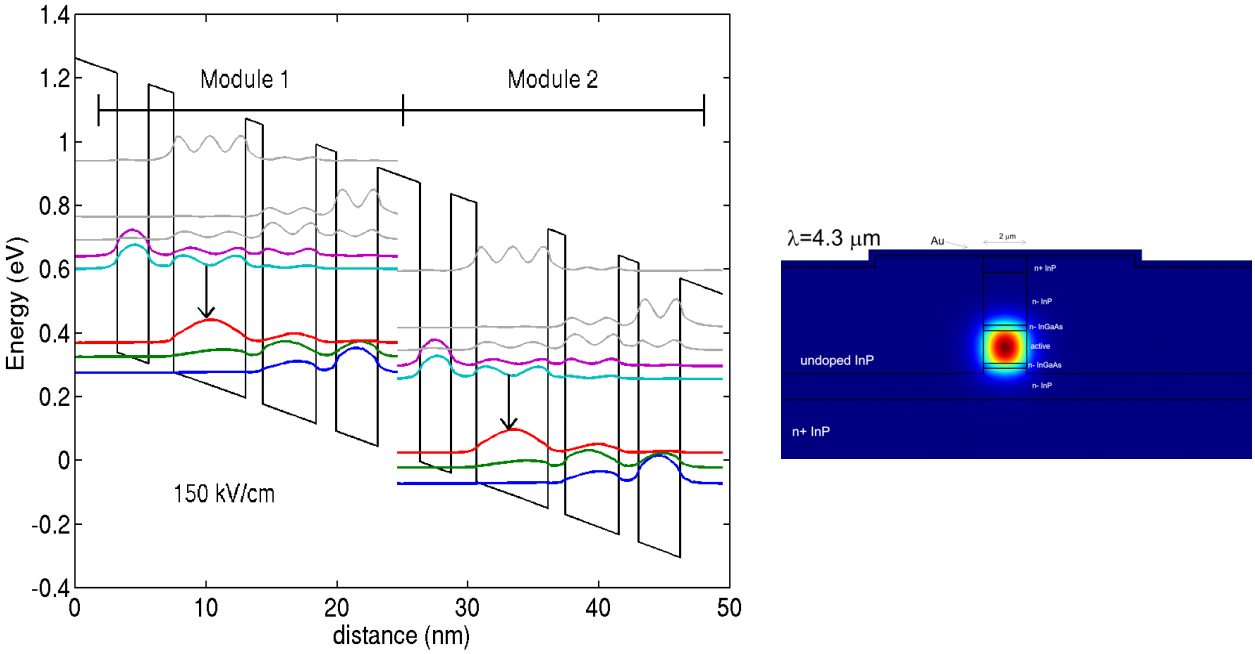

Figure 21. Left: Band diagram and wavefunctions of a quantum-cascade laser at 4.7 μm wavelength with only 4 wells per module. Right: Mode profile of a narrow (2 μm) laser ridge with regrown InP cladding layer and top Au layer.

At end of the first year of this project, our team has developed QCLs operating near 4.7-μm wavelength at room temperature in continuous-wave (CW) mode. The CW power-current and voltage-current curves at different temperatures are shown in Fig. 21. This rapid development is encouraging for military and biochemical sensing applications.

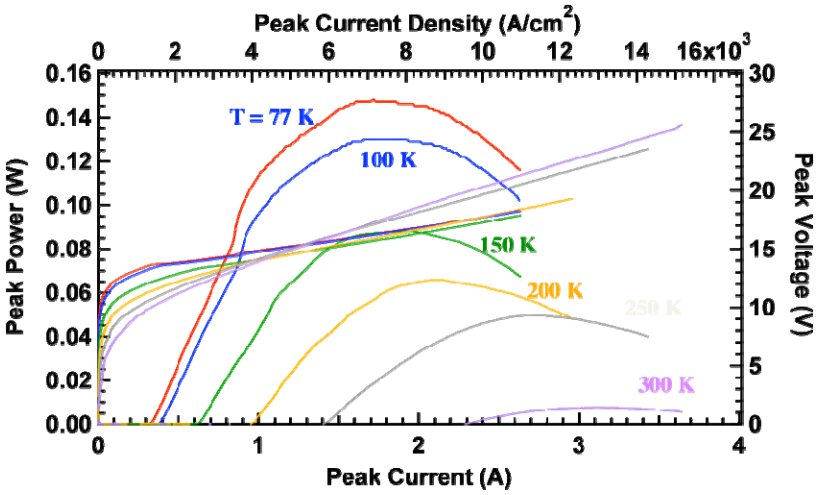

Figure 22. Power-current and voltage-current relations of an injectorless quantum-cascade laser up to room temperatures.

Patent applications, Publications, and Conference Presentations

- Sushil Kumar and Alan W. M. Lee, "Resonant-Phonon Terahertz Quantum-Cascade Lasers and Video-Rate Terahertz Imaging," IEEE Journal of Quantum Electronics, **14**, 333 (2008). (Invited)

- S. Kumar, A. W. M. Lee, Q. Qin, B. S. Williams, Q. Hu, and J. L. Reno, "High-temperature and high-power operation of terahertz quantum-cascade lasers," SPIE Proceedings (2008).

- G. Scamarcio, M. S. Vitiello, V. Spagnolo, S. Kumar, B. S. Williams, and Q. Hu, "Nanoscale heat transfer in quantum cascade lasers," Physica E **40**, 1780 (2008).

- Wade, G. Fedorov, D. Smirnov, S. Kumar, B. S. Williams, Q. Hu, and J. L. Reno, "Magnetic-field-assisted terahertz quantum cascade laser operating up to 225 K," Nature Photonics, **3**, 41 (2009).

- Q. Hu, “Quantum warming,” cover interview, Nature Photonics, **3**, 64 (2009).

- P. Khosropanah, A. Baryshev, W. Zhang, W. Jellema, J.N. Hovenier, J.R. Gao, T.M. Klapwijk, D.G. Paveliev, B. S. William, S. Kumar, Q. Hu, and J. L. Reno, “Phase-locking of a 2.7-THz quantum cascade laser to a microwave reference,” submitted to Opt. Lett. (2009).

- S. Kumar, Q. Hu, and J. L. Reno, “186 K operation of THz quantum cascade lasers based on a diagonal design,” Appl. Phys. Lett. **94**, 131105 (2009).

- J. Gambari, S. A. Maier, B. S. Williams, S. Kumar, J. L. Reno, Q. Hu, and C. C. Phillips, “Thresholdless lasing from a semiconductor nanostructure in a strongly coupled microcavity,” submitted to Nature Photonics, (2009).

- Q. Qin, B. S. Williams, S. Kumar, J. L. Reno, and Q. Hu, “Tuning a Terahertz Wire Laser,” submitted to Nature Photonics (2009).

- Qing Hu and Benjamin S. Williams, "Terahertz Lasers and Amplifiers Based on Resonant Optical Phonon Scattering to Achieve Population Inversion," U. S. Patent No. 7,548,566, issued on June 16, 2009.

- S. Kumar, C. W. I. Chan, Q. Hu, and J. L. Reno, “Two-well terahertz quantum-cascade laser with direct intrawell-phonon depopulation,” submitted to Appl. Phys. Lett. (2009).

- S. Kumar and Q. Hu, “Coherence of resonant-tunneling transport in terahertz quantum-cascade lasers,” submitted to Phys. Rev. **B** (2009).

- S. Kumar, A. W. M. Lee, Q. Qin, B. S. Williams, Q. Hu, and J. L. Reno, "High-temperature and high-power operation of terahertz quantum-cascade lasers," IEEE Phonoics West, San Jose, CA, 19 - 24 January (2008). (Invited)

- Q. Hu, "Resonant phonon-based THz quantum-cascade lasers and real-time T-rays imaging", International Quantum Cascade Lasers School & Workshop Monte Verita, Switzerland, September 14-19 (2008). (Invited)

- S. Kumar, Q. Hu, and J. L. Reno, "Bidirectional Terahertz Quantum-Cascade Lasers", International Quantum Cascade Lasers School & Workshop Monte Verita, Switzerland, September 14-19 (2008).

- Alan W.M. Lee, Sushil Kumar, Ben Williams, Qing Hu, and John L. Reno, "Tunable THz QCLs", International Quantum Cascade Lasers School & Workshop Monte Verita, Switzerland, September 14-19 (2008).

- Q. Hu, "Terahertz Quantum Cascade Lasers and Real-time THz Imaging ", International Workshop "THz Radiation: Basic Research and Applications" (TERA 2008), Alushta, Crimea, Ukraine, October 2 - 4, (2008). (Invited)

- A. Wade, G. Fedorov, D. Smirnov, S. Kumar, Q. Hu, B. S. William, "Magnetic field controlled sub-THz emission in Quantum Cascade Lasers," APS March Meeting, March (2008).

- Q. Hu, "Terahertz Quantum Cascade Lasers and Real-time THz Imaging," SUNY at Buffalo EE colloquium, October 23 (2008).

- Q. Hu, "THz Quantum Cascade Lasers and sub-surface T-rays Imaging at Video Rate," Terahertz Imaging and Spectroscopy Workshop, Northeastern University, Boston, October 30 (2008). (invited)

- Q. Hu, “Terahertz quantum cascade lasers and video-rate THz imaging,” International Workshop on Optical Terahertz Science and Technology 2009 (OTST 2009), Santa Barbara, CA, March 7-11, (2009). (Invited)

- S. Kumar, Q. Hu, J. L. Reno, “Low-Threshold Terahertz Quantum-Cascade Lasers with One-Well Injector Operating up to 174K,” CLEO/IQEC 2009, CThH4, Baltimore, Maryland, June 4 (2009).

- Alan W. M. Lee, Q. Qin, S. Kumar, Q. Hu, J. L. Reno, “Frequency-Tunable External Cavity Terahertz Quantum Cascade Laser,” CLEO/IQEC 2009, CThH5, Baltimore, Maryland, June 4 (2009).

- Allen L. Hsu, Q. Hu, and B. S. Williams, “Four-Well Highly Strained Quantum Cascade Lasers Grown by Metal-Organic Chemical Vapor Deposition,” CLEO/IQEC 2009, CThL2, Baltimore, Maryland, June 4 (2009).

- Q. Hu, “Terahertz quantum cascade lasers and video-rate THz imaging,” 2009 Advanced Research Workshop (FTM-6), Future Trends in Microelectronics: Unmapped Roads, Sardinia, Italy, June 14-19 (2009). (Invited)

- Q. Hu, “Terahertz quantum cascade lasers and video-rate THz imaging,” Device Research Conference (DRC), Penn State University, June 22-24, (2009). (Invited)

- Sushil Kumar, I. Chan, Q. Hu, and J. L. Reno, “Terahertz Quantum-Cascade Lasers with Resonant-Phonon Depopulation,” the 10th International Conference on Intersubband Transitions in Quantum Wells (ITQW'09), Montreal, Canada, September 6-11 (2009). (Invited)

- 140. P. Khorsropanah, A. Baryshev, W. Zhang, W. Jelleman, J. N. Hovenier, J. R. Gao, T. M. Klapwijk, D. G. Paveliev, S. Kumar, B. S. Williams, Q. Hu, J. L. Reno, B. Klein, and J. L. Hesler, “Phase-locking of a 2.7-THz quantum cascade laser to a microwave reference,” the 10th International Conference on Intersubband Transitions in Quantum Wells (ITQW'09), Montreal, Canada, September 6-11 (2009).

- C. A. Wang, A. K. Goyal, R. K. Huang, J. P. Donnelly, D. R. Calawa, G. W. Turner, A. Sanchez-Rubio, A. Hsu, Q. Hu, and B. S. Williams, “GaInAs/AlInAs/InP Quantum Cascade Laser Materials,” the 17th American Conference on Crystal Growth and Epitaxy (17th ACCGE), Lake Geneva, Wisconsin, August 9-14 (2009).

- Q. Hu, " Tunable and high-temperature THz quantum-cascade lasers", IEEE Phonoics West, San Francisco, CA, January 23-28 (2010). [ ] (Invited)

M.S. thesis

Allen Long Hsu, “Design of High Efficiency Mid IR QCL Lasers”. August, 2008.